Pis'ma v ZhETF, vol. 99, iss. 1, pp. 30 – 34 © 2014 January 10

Ultrafast optical probes of dynamic behavior in $La_{0.7}Sr_{0.3}MnO_3/YBa_2Cu_3O_{7-\delta}/La_{0.7}Sr_{0.3}MnO_3$ heterostructure

L. Peng[1)], *Ch. Cai*[+], *D. H. Xu*, *Y. Liu*

Department of Physics, Shanghai University of Electric Power, 201300 Shanghai, China

[+]*Department of Physics, Shanghai University, 200444 Shanghai, China*

Submitted 28 October 2013

Resubmitted 9 December 2013

Ultrafast pump-optical probe spectroscopy was used to analyze carriers dynamics behavior in $La_{0.7}Sr_{0.3}MnO_3/YBa_2Cu_3O_{7-\delta}/La_{0.7}Sr_{0.3}MnO_3$ heterostructure. Our results show the pump signal $\Delta R/R$ for higher laser power (such as 21 and 41 mW), below T_c, first goes positive, then crosses zero and goes negative, before relaxing back to equilibrium over a time scale of a few ten picoseconds. We extract the characteristic relaxation time of the different process by fitting the data at these powers with a three-exponential decay. For higher laser power, the long characteristic relaxation time are obtained, which implies the competition between FM order and SC order in the $La_{0.7}Sr_{0.3}MnO_3/YBa_2Cu_3O_{7-\delta}/La_{0.7}Sr_{0.3}MnO_3$ heterostructure.

DOI: 10.7868/S0370274X14010068

1. Introduction. The study of hybrid structures composed of superconductor (SC) and ferromagnet (FM) systems have revealed a variety of exotic phenomena in these systems [1–13]. Several spin-dependent transport effects such as magnetoresistance effect [13] in FM/SC/FM trilayers, π-shift in SC/FM/SC Josephson junctions [14, 15], oscillations of T_c with the FM layer thickness [16] and inverse proximity effect in FM/SC bilayer structures [17], inverse spin switch effect in superconducting spin valves [18], and spin-triplet Josephson effect were recently observed in FM/SC multilayers [19]. Most research in this field has involved single element or alloy-based metallic superlattices. The extension of concepts of the FM/SC proximity effect to the high-T_c superconductors or colossal magnetoresistance oxide is of primary interest since peculiarities like the short superconducting coherence length and full spin polarization could open the door to interesting new effect.

Recently, researchers have paid extensive attention to investigate the strongly correlated electron materials by the ultrafast techniques since the relative contributions of electron, phonon, and spin dynamics in these materials can be directly resolved in the time domain [20–23]. Moreover, the temperature dependence of the relaxation behavior always exhibits a dramatic change near the transition temperature, which may reveal the valuable information about the physical mechanisms governing the intriguing properties of these materials. Therefore, femtosecond time-resolved spectroscopy has been recognized as a powerful technique to study temperature dependent changes of the low-lying electron structure of superconductors [22] and other strongly correlated electron materials [23]. It providers a new avenue, namely, the time domain, for understanding the quasiparticle excitations of these materials. In our work, the magnetic properties and excited carrier dynamics of $La_{0.7}Sr_{0.3}MnO_3/YBa_2Cu_3O_{7-\delta}/La_{0.7}Sr_{0.3}MnO_3$ heterostructure are investigated with time-resolved optical pump probe method.

2. Experiments. A typical pulsed laser deposition (PLD) system equipped with multiple targets and an excimer laser (the wavelength is 248 nm) was used to grow the heterostructure on the substrate of single crystal $LaALO_3$ (LAO). The laser repetition rate and substrate temperature are fixed at 4 Hz, and 800 °C, respectively. The pulsed laser energy density was around 2.5 J/cm^2. Oxygen partial pressures of 400 mTorr for $La_{0.7}Sr_{0.3}MnO_3$ (LSMO) and 250 mTorr for $YBa_2Cu_3O_{7-\delta}$ (YBCO) were applied during the thin film growth. Further details about growth and structure can be found elsewhere [11, 12]. With these parameters, a 50 nm LSMO layer was deposited first on (100) LAO substrate. Then a 50 nm YBCO layer, and 50 nm LSMO layer were deposited subsequently.

The heterostructure was characterized by X-ray diffraction (XRD) (D\max-2200). The electric transport measurements of the studied film was made by four-contact and current contacts were in the plane of the film (current in-plane geometry). Magnetic properties of

[1)]e-mail: plpeng@shiep.edu.cn

the heterostructure were investigated by magnetization–temperature (M–T) and magnetization–applied field (M–H) measurements using a cryostat equiped with a 9 T magnet (Quantum Design PPMS-9 T).

Time-resolved optical spectroscopy was performed using pump and probe pulses. A high peak-power laser beam centred at 800 nm was delivered from a regenerative Ti: sapphire amplifier using chirped pulse amplification technique (RegA9000, Coherent Inc.). The output pulse with a pulse width of 120 femtosecond and repetition rate of 250 kHz was frequency-double in a 0.5 mm long nonlinear optics β-BaB_2O_4 (BBO) crystal to generate 400 nm pulse beams. A two-colour laser beam was divided into two beams by a dichroic mirror. The transmitted second harmonic generation (SHG) beam (centred at 400 nm) was used as pump beam, which was chopped at a frequency of 1320 Hz and passed through an optical delay driven by a computer-controlled step motor. The reflected fundamental beam was used as probe beam, and the two beams were focused on by a 10cm-focal-length lens and over lapped on the same spot of the sample with a spot size of 100 μm. After passing through the sample, the pump beam was blocked with a non-transparent aperture, while the probe beam was guided to a photodiode connected to a lock-in amplifier.

3. Results and discussions. The XRD patterns of LSMO/YBCO/LSMO are depicted in Fig. 1. The pres-

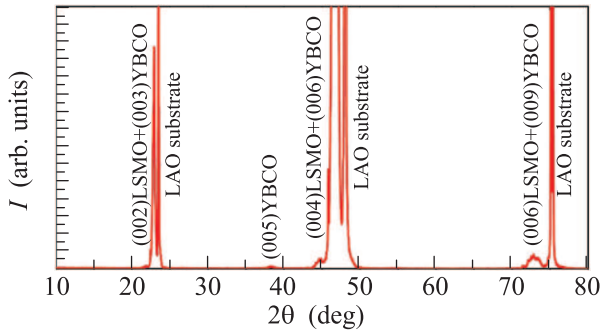

Fig. 1. (Color online) X-ray diffraction pattern of LSMO/YBCO/LSMO heterostructure

ence of only (00l) lines suggests that the heterostructure are grown with the c-axis perpendicular to the substrate surface.

Fig. 2 shows the M–T curves of LSMO/YBCO/LSMO under ZFC and FC modes. Based on the M–T curves, the superconducting critical temperature T_c for the studied sample is determined as 74 K which is 14 K lower than that of YBCO film ($T_{sc} = 88$ K). And the electrical transport measurement for pure YBCO is also made and the superconducting transition temperature is 88 K.

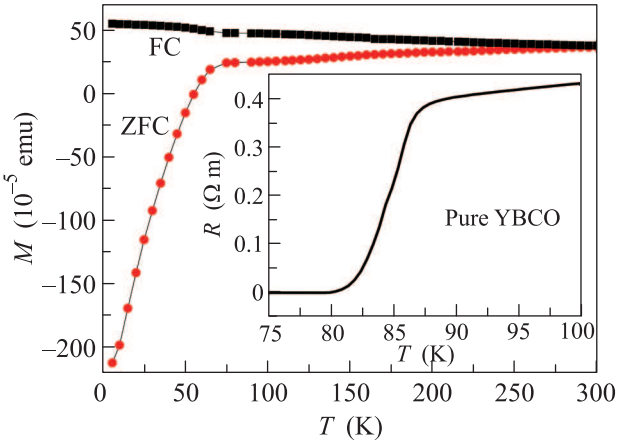

Fig. 2. (Color online) ZFC and FC magnetic moment (M) versus temperature (T) of LSMO/YBCO/LSMO heterostructure for magnetic field parallel to c-axis. The inset shows the resistivity versus temperature curve in zero field for pure YBCO film

Displayed in Fig. 3 is the magnetic hysteresis loops measured on the studied heterostructure at $T = 50$ and 10 K in magnetic fields applied both parallel and perpendicular to the film plane. The out-of-plane M–H curve shows a well defined hysteresis loop, which is associated with the diamagnetic behavior of the superconducting layer. In turn, the in-plane M–H curve displayers the typical ferromagnetic hysteresis loop corresponding to a single F layer. The clear observation of this magnetic anisotropic behavior speaks for the high quality of the heterostructure and the close interplay between the superconducting and ferromagnetic phases.

The transient reflectivity $\Delta R/R$ spectra of the LSMO/YBCO/LSMO as measured by a conventional pump-probe method are shown in Fig. 4. An amplified mode-locked Ti:sapphire laser with the repletion rate of 1 kHz and the central wavelength of 800 nm (1.55 eV) was used for the pump light source. At high T the signal is characterized by a $\Delta R/R$ transient relaxation which $\tau_n \sim 4.09$ ps with τ_n increasing slightly as $T > T_c$ ($T_c = 74$ K) (see the Fig. 4). Accordingly, it is noted that the $\Delta R/R$ curves exhibit damped oscillations. The damped oscillations in the $\Delta R/R$ curves, originally identified by Thomsen et al. [24], have been ascribed to the coherent longitudinal acoustic phonon oscillations generated by the interference of the probe beams reflected from the interfaces defined by the crystal surface and the layer of propagating strain pulse. Below T_c, we observe the rapid enhancement of the signal $\Delta R/R$ with a characteristic relaxation time $\tau_c \sim 4.11$ ps at the opening of the SC gap Δ. However, we don't observe clearly the relaxation process of two mutually competing orders.

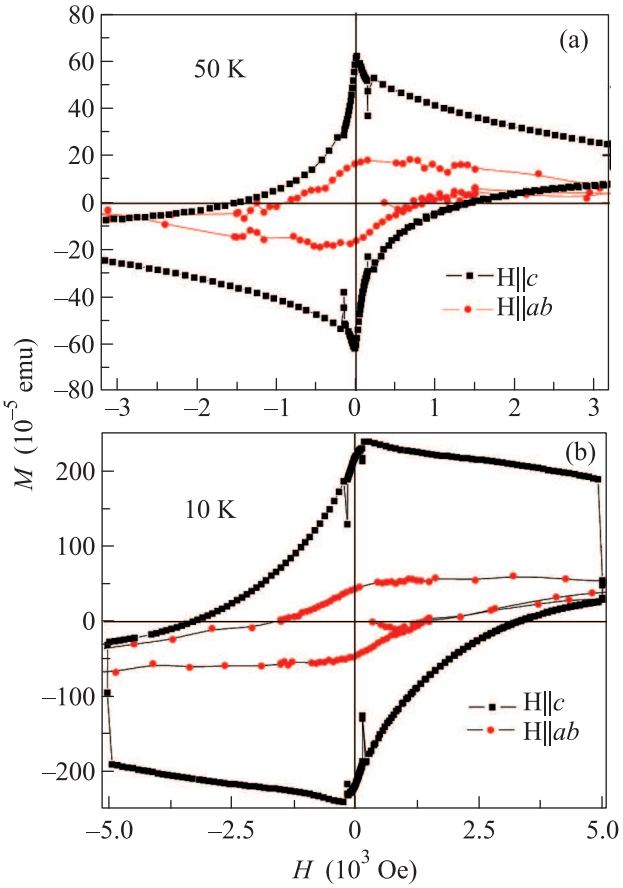

Fig. 3. (Color online) $M-H$ hesteresis loops of LSMO/YBCO/LSMO heterostructure recorded at 50 and 10 K with the magnetic field applied both perpendicular and parallel to the plane of LSMO/YBCO/LSMO heterostructure

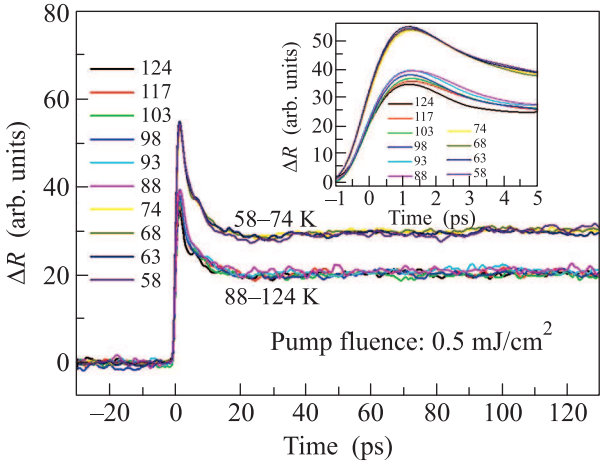

Fig. 4. (Color online) Photoinduced transient reflection $\Delta R/R$ vs time delay between pump and probe pulses at the range of 58–124 K. Inset: region expanded near the peak position

The laser energy used during our experiment could be too low to completely destroy the superconducting order and the second ferromagnetic order, and the competition between the superconducting order and the ferromagnetic order is not clearly observed. Fig. 5a shows

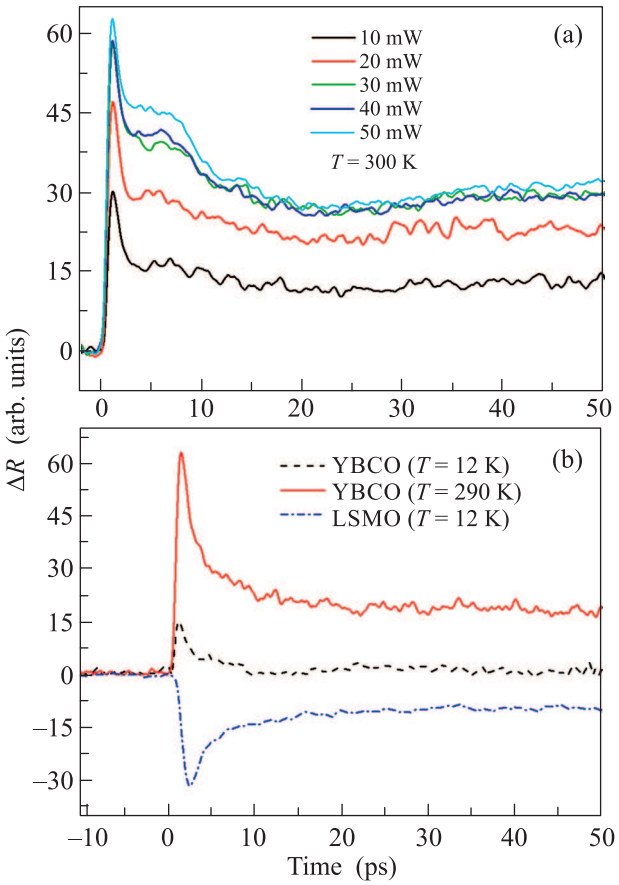

Fig. 5. (Color online) (a) – Time dependence of the circular pump signal at different laser power and $T = 300$ K. (b) – Photoinduced transient reflection $\Delta R/R$ vs time delay for YBCO at $T = 12$ K and 290 K and LSMO at $T = 12$ K. The pump power is 40 mW

the time dependence of the pump signal at different laser power and $T = 300$ K. We observe the like-plaute effect at high laser power (such as 30 mW) from the signal $\Delta R/R$ curves, which indicates the photoexcitation and retrapping process of the correlated polarons in the ferromagnetic phase and paramagnetic phase due to heat-exciting. For comparison, we study the the signal $\Delta R/R$ curves for the superconductor, the superconductor in normal state and the single ferromagnetic layer (see Fig. 5b). We also fit the new data of $\Delta R/R$ and obtain the decay time 4.55, 3.77, and 6.96 ps for the superconductor, the superconductor in normal state and the single ferromagnetic layer, respectively. On the other hand, below T_c (such as 12 K), the pump signal $\Delta R/R$

for higher power 21 and 41 mW (see the Fig. 6) first goes

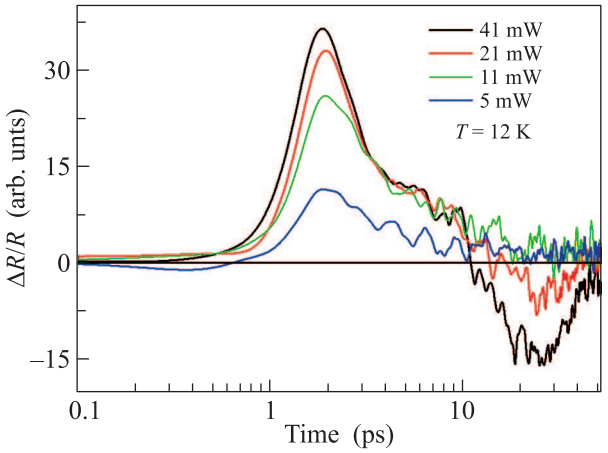

Fig. 6. (Color online) Time dependence of the pump signal at different laser power and $T = 12\,\mathrm{K}$

positive, then crosses zero and goes negative, before relaxing back to equilibrium over a time scale of a few picoseconds. We ascribe the short-decay positive signal to the reformation of SC order following photo-excitation and the long-decay negative signal to the development of a competing FM order according to the Fig. 5b. Accordingly, we fit the data of $\Delta R/R$ in different power ranges as follows: for the lower laser power, the data follow

$$\Delta R/R = A_0 + A_1 \exp(-t/\tau_1), \qquad (1)$$

where $\tau_1 \sim 7.8\,\mathrm{s}$ for power 11 mW and $\tau_1 \sim 9.1\,\mathrm{ps}$ for power 5 mW. For higher power, the data follow

$$\Delta R/R = A_0 + A_1 \exp(-t/\tau_1) + \\ + A_2 \exp(-t/\tau_2) + A_3 \exp(-t/\tau_3), \qquad (2)$$

where $\tau_1 = 22.56\,\mathrm{ps}$, $\tau_2 = 25.67\,\mathrm{ps}$, and $\tau_3 = 22.51\,\mathrm{ps}$ for power 41 mW, $\tau_1 = 16.07\,\mathrm{ps}$, $\tau_2 = 15.75\,\mathrm{ps}$, and $\tau_3 = 17.21\,\mathrm{ps}$ for power 21 mW. For higher laser power, the long characteristic relaxation time are obtained. The first term shows the reformation of SC order of YBCO. The second term shows the competition between FM order and SC order and the reformation of FM order. The last term corresponds to the quasiparticle thermalization and electron-hole pair recombination. We could use the Rothwarf–Taylor (RT) model to explain our data [25]. It is a phenomenological model used to describe the relaxation of photo-excited SCs, where the presence of a gap in the electronic density of states gives rise to a bottleneck for carrier relaxation. When two quasi-particles with energies $\varepsilon \geq \Delta$ recombine, a high-frequency boson (HFB) with energy $\varepsilon \geq 2\Delta$ is created. The HFBs that remain in the excitation volume can subsequently break additional Cooper pairs effectively inhibiting quasi-particle recombination. SC recovery is governed by the decay of the HFB population.

4. Conclusions In summary, we used ultrafast pump-optical probe spectroscopy to analyze the carriers dynamics behavior in LSMO/YBCO/LSMO heterostructure. The time dependence of photoexcitation and the subsequent relaxation of correlated carriers reveal the dynamics process of two mutually competing orders in the studied system. The present study demonstrates that ultrafast pump-optical probe spectroscopy can serve as an alterative experimental technique to investigate the dynamics behavior of FM/SC heterostructures, which is crucial for understanding the exotic physical properties of these systems.

This work is sponsored by the Natural Science Foundation of Shanghai (# 13ZR1417600), the Innovation Program of Shanghai Municipal Education Commission (# 14YZ132), the National Natural Science Foundation of China (# 11374204), the Science and Technology Commission of Shanghai Municipality (# 12JC1404400, 11160500700), and the Shanghai Science Fund for the Excellent Young Teachers (# Z2012-012).

1. P. Grünberg, R. Schreiber, Y. Pang, M. B. Brodsky, and C. H. Sowers, Phys. Rev. Lett. **57**, 2442 (1986).
2. M. N. Baibich, J. M. Broto, A. Fert, F. Nguyen van Dau, F. Peoff, P. Etienne, G. Creuzet, A. Friederich, and J. Chazeles, Phys. Rev. Lett. **61**, 2472 (1988).
3. G. Sun, D. Y. Xing, and J. Dong, Phys. Rev. B **65**, 174508 (2002).
4. T. Kontos, M. Aprili, J. Lesueur, and X. Grison, Phys. Rev. Lett. **86**, 304 (2001).
5. V. A. VasTko, V. A. Larkin, P. A. Kraus, K. R. Nikolaev, D. E. Grupp, C. A. Nordman, and A. M. Goldman, Phys. Rev. Lett. **78**, 1134 (1997).
6. N. C. Yeh, R. P. Vasque, C. C. Fu, A. V. Samoilov, Y. Li, and K. Valiki, Phys. Rev. B **60**, 10522 (1999).
7. J. Y. T. Wei, J. Supercond. **15**, 67 (2002).
8. M. D. Allsworth, R. A. Chakalov, M. S. Colclough, P. Mikheenko, and C. M. Muirhead, Appl. Phys. Lett. **80**, 4196 (2002).
9. Z. Sefrioui, M. Varela, V. Pena, D. Arias, C. Leon, J. Santamaria, J. E. Villegas, J. L. Martinez, W. Saldarriaga, and P. Prieto, Appl. Phys. Lett. **81**, 4568 (2002).
10. L. Peng, C. Cai, C. Chen, Z. Liu, R. Hühne, and B. Holzapfel, J. Appl. Phys. **104**, 033920 (2008).
11. L. Peng, C. Cai, C. Chen, F. Fan, X. Wang, and Z. Liu, J. Appl. Phys. **105**, 073908 (2009).
12. L. Peng, C. Cai, C. Chen, B. Gao, L. Ying, and Z. Liu, Sol. Stat. Comm. **148**, 545 (2008).
13. V. Peña, Z. Sefrioui, D. Arias, C. Leon, and J. Santamaria, Phys. Rev. Lett. **94**, 057002 (2005).

14. Z. Radovic, M. Ledvij, L. Dobrosavljevic-Grujic, A. I. Buzdin, and J. R. Clem, Phys. Rev. B **44**, 759 (1991).
15. T. Muhge, N. N. Garifyanov, Y. V. Goryunov, G. G. Khaliullin, L. R. Tagirov, K. Westerholt, I. A. Garifullin, and H. Zabel, Phys. Rev. Lett. **77**, 1857 (1996).
16. I. C. Moraru, W. P. Pratt. Jr, and N. O. Birge, Phys. Rev. Lett. **96**, 037004 (2006).
17. J. Xia, V. Shelukhin, M. Karpovski, A. Kapitulnik, and A. Palevski, Phys. Rev. Lett. **102**, 087004 (2009).
18. J. Zhu, X. Cheng, C. Boone, and I. N. Krivorotov, Phys. Rev. Lett. **103**, 027004 (2009).
19. L. Trifunovic, Z. Popovic, and Z. Radovic, Phys. Rev. B **84**, 064511 (2011).
20. Y. H. Ren, H. B. Zhao, G. Lüpke, C. S. Hong, N. H. Hur, Y. F. Hu, and Q. Li, J. Chem. Phys. **121**, 436 (2004).
21. Y. H. Ren, M. Ebrahim, H. Zhao, G. Lüpke, Z. A. Xu, V. Adyam, and Q. Li, Phys. Rev. B **78**, 014408 (2008).
22. E. E. M. Chia, J. Zhu, D. Talbayev, R. D. Averitt, and A. J. Taylor, Phys. Rev. Lett. **99**, 147008 (2007).
23. K. H. Wu, T. Y. Hsu, H. C. Shilh, Y. J. Chen, C. W. Luo, T. M. Uen, J.-Y. Lin, J. Y. Juang, and T. Kobayashi, J. Appl. Phys. **105**, 043901 (2009).
24. C. Thomsen, H. T. Grahn, H. J. Maris, and J. Tauc, Phys. Rev. B **34**, 4129 (1986).
25. A. Rothwarf and B. N. Taylor, Phys. Rev. Lett. **19**, 27 (1967).